IEEE Access
Multidisciplinary | Rapid Review | Open Access Journal

Received April 29, 2022, accepted May 11, 2022, date of publication May 16, 2022, date of current version May 23, 2022.

Digital Object Identifier 10.1109/ACCESS.2022.3175460

Breakdown of Synthetic Air Under Nanosecond Pulsed Voltages in Quasi-Uniform Electric Fields

MICHELANGELO BALMELLI[1,2], YANG LU[1,3], RAPHAEL FÄRBER[3], LAURA MEROTTO[1], PATRIK SOLTIC[1], (Member, IEEE), DAVIDE BLEINER[1,4], JÜRGEN BIELA[2], (Senior Member, IEEE), AND CHRISTIAN M. FRANCK[3], (Senior Member, IEEE)

[1]Empa, Swiss Federal Laboratories for Materials Science and Technology, 8600 Dübendorf, Switzerland
[2]Laboratory for High Power Electronic Systems, ETH Zürich, 8092 Zürich, Switzerland
[3]High Voltage Laboratory, ETH Zürich, 8092 Zürich, Switzerland
[4]Department of Chemistry, University of Zurich, 8057 Zürich, Switzerland

Corresponding author: Michelangelo Balmelli (michelangelo.balmelli@empa.ch)

This work was supported by the Swiss Federal Office of Energy (Research on Alternative Combustion Concepts for Efficient Gas Engines) under Contract SI/501755-01.

ABSTRACT The electrical breakdown of synthetic air under ultrashort high-voltage pulses (50 ns duration), as well as slowly increasing (''DC'') voltages, is experimentally studied in a well-defined quasi-uniform electrode configuration (sphere–plane). The electrode spacing is varied from 0.1 to 1 mm, and the gas pressure is varied from 1.5 to 8 bar. The study's goal is to provide experimental data to develop breakdown models that predict the breakdown probability of small gas gaps under arbitrary voltage excitations. In particular, this analysis is intended for applications where statistical and formative time lags need to be considered, such as nanosecond pulsed ignition or partial discharges in inverter-fed motors. The influence of the electrode material and the presence of UV illumination are investigated for both DC and pulsed voltages. The results highlight the important role of seed electron provision for breakdown under short transient voltages. Evidence for a field-assisted emission of seed electrons with a pressure-dependent onset field is found from time lag measurements. An empirical expression is derived based on the Fowler–Nordheim formula to quantify the seed electron generation rate. The expected dependence of the breakdown threshold on the cathode material (work function) was confirmed for breakdown under slowly increasing voltages (Townsend mechanism). Interestingly, a dependence of the breakdown voltage was also found for nanosecond pulsed voltages (dominated by the streamer mechanism). This suggests that the field emission of electrons from the cathode is the dominant source of seed electrons in large cathode electric fields.

INDEX TERMS Breakdown, nanosecond pulsed discharge, ignition, nanosecond repetitive pulsed discharge, NRPD, nonequilibrium plasma, pulsed discharge, spark-ignition engines, seed electrons, streamer, townsend.

I. INTRODUCTION

The electrical breakdown of gases under nanosecond high-voltage transients is of great interest for various technical applications. In some applications, such as chemical plasma reactors [1], plasma surface treatments [2], or spark ignition systems [3], the creation of plasma is the desired outcome. In other applications, such as insulation systems for inverter-fed motors and transformers, repetitive nanosecond high-voltage transients can occur during the switching process and ignite an undesired plasma in gas gaps bounded by solid insulation materials. Usually of a transient nature, these *partial discharges* (discharges that do not completely bridge the space between the two conductors) cause chemical and physical erosion of the solid insulation, which is the leading cause of premature insulation failures in inverter-driven systems [4].

In spark-ignition engines, the ignition process often limits increased efficiency and the range of usable excess air or exhaust gas recirculation [5]. In conventional ignition

The associate editor coordinating the review of this manuscript and approving it for publication was Guillaume Parent.

systems for engines, a spark (thermal plasma channel) is used to initiate fuel combustion [3]. Some of the mentioned limitations can be overcome by using repetitive voltage pulses of some tens of nanoseconds duration, which allow the initiation of breakdown at higher voltages and thus channel more energy into the phase where the plasma is not in thermal equilibrium. The resulting advantages are shorter ignition delays, stable ignition at higher air-to-fuel ratios or exhaust gas dilution, and faster flame propagation [6]–[8]. Computational fluid dynamic modeling of ignition from a nanosecond pulsed discharge was reported in [9], and a description of the energy delivered during the discharge was reported in [10]; nevertheless, the characterization and modeling of breakdown thresholds (e.g., probability of breakdown occurring for a pulse of given amplitude, rise time, and duration) and the distribution of delay times are lacking.

The influence of the nanosecond pulse rise rate on the breakdown voltage and breakdown time was investigated in [11]. Two pulse durations of 50 and 10 ns were used, and streamer theory was identified as the breakdown onset mechanism. Due to the fast but finite pulse rise time, the authors measured significantly different breakdown voltages and times for varying pulse rise rates. In the investigation, the minimal observed breakdown delay time was used as an upper bound for the formative time. The presented analysis showed that the statistical time lags decrease with increasing overvoltages. Moreover, the seed electron generation rate, which primarily determines the statistical time lag, was found to strongly increase at large fields, but a quantitative analysis of the seed electron rate was difficult, because the study used automotive sparkplugs where the electrode geometry is complex and nonuniform. In such a geometry, estimating the active cathode area, for which an electron appearing near the cathode can induce breakdown, is complex and subject to considerable uncertainties.

This study aims to provide and analyze similar experimental data but for a simplified electrode geometry (sphere–plane, quasi-uniform electric field, as shown in Figure 2), for which the seed electron generation rate can be determined more accurately by using the calculated active cathode area. The provided parametrization of the seed electron rate as a function of the gap electric field and pressure is a novel contribution of this paper, which can be used to develop models for breakdown under nanosecond transients.

Breakdown thresholds for DC voltage are also measured under the same conditions of gap distance and pressure to allow for direct comparison and normalization of the transient breakdown voltages. For both the transient and DC voltages, the effect of the electrode material and UV illumination of the cathode are investigated to obtain information about the presence of secondary feedback and the role of seed electron provision.

As the timescale of the voltage application drops to the same order of magnitude as the statistical delay, the seed electron generation rate is expected to have a significant impact on the observed breakdown voltage. A clearer physical picture and a quantitative description of the seed electron generation mechanism in small gaps are thus required. This paper will contribute to the understanding of the breakdown in small gaps under nanosecond high-voltage pulses by providing an empirical expression for the seed electron generation rate as a function of the gap electric field.

The organization of the paper is as follows. First, the theory of the electrical breakdown of gases is summarized, focusing on the factors affecting the time to breakdown when fast-rising voltages are applied. Then, the experimental setup used in this investigation is presented alongside the simulation of the electric field of the used geometry. The results are divided into three parts. First, the results under slowly increasing (DC) voltage are presented. In the second part, the experiments under pulsed breakdown voltages are explained and compared to the DC results. Finally, the times to breakdown under pulsed voltages are analyzed, and an empirical expression for the seed electron generation rate is proposed. The presented results are then discussed and summarized based on gas discharge theory.

II. METHODS

A. THEORY

The electrical breakdown of a gas gap starts with one or more free electrons – so-called *seed electrons* – that gain kinetic energy from the applied electric field. Seed electron generation is a stochastic process and leads to a fluctuating breakdown delay known as the *statistical time lag* [12], [13]. If the field magnitude exceeds the gas's *critical field strength*, an electron avalanche can result from the impact ionization of neutral gas molecules. According to the streamer mechanism, a direct breakdown can occur if the electron number in an avalanche grows to $10^6 \ldots 10^8$ electrons. If so, a direct breakdown without cathode feedback can occur according to the *streamer mechanism* [14]. Alternatively, breakdown may occur as a result of a growing number of secondary avalanches starting from electrons liberated from the cathode by energetic input (positive ions, photons, metastable atom, etc.) from previous avalanches (*Townsend mechanism*). The two mechanisms are described in more detail in the following subsection.

1) BREAKDOWN MECHANISMS

The gas breakdown mechanisms depend on the time-varying electric field and on the seed electron provision. In this investigation, a geometry providing a quasi-uniform electric field is chosen. The gas contains relatively few free charged particles and is thus a good electrical insulator. However, if the electrical field is high enough, positive ions, photons, or excited neutral molecules created in an avalanche can reach the cathode surface and release secondary electrons (if they can impart with an energy exceeding the *work function* of the cathode surface to the electrons). This feedback process is quantified by the *secondary feedback emission coefficient* (γ), which is defined as the number of secondary

electrons released per ionization event in an avalanche. In each avalanche generation, the number of electrons is enhanced by the *amplification factor* μ given by Equation (1).

$$\mu = \gamma \cdot e^{\int_0^d \alpha_{\text{eff}} \cdot \text{dx}} = \gamma \cdot e^{S} \tag{1}$$

According to Townsend theory, a breakdown occurs when each avalanche creates, on average, more than one successor avalanche, that is, when $\mu > 1$. The corresponding *Townsend criterion* thus reads

$$S = \int_0^d \alpha_{\text{eff}} \cdot \text{dx} = \int_0^d \alpha - \eta \cdot \text{dx} = \ln\left(\gamma^{-1}\right) \tag{2}$$

The integral S is called the *ionization integral* and equals the line integral of the *effective ionization coefficient* (α_{eff}) along a considered field line across the gas gap. The term α_{eff} considers the effects of both *ionization* (α) and *attachment* (η) of electrons.

If the Townsend criterion is fulfilled, the number of avalanches in subsequent generations will increase exponentially until a certain critical number $E_a \approx 10^6 \ldots 10^{10}$ of avalanches is formed, where space charge effects start to dominate the subsequent dynamics of the breakdown [15]. The formative time of Townsend breakdown, i.e., the time required to build up E_a avalanches, can be estimated by Equation (3), where v_e is the *drift velocity* of electrons (see Appendix A for the derivation).

$$t_{\text{f,T}} = \frac{\ln\left[(\mu - 1)\, E_a\right]}{\ln \mu} \cdot \left[\tau_1 + \left(1 - \frac{1}{\alpha_{\text{eff}} \cdot d}\right) \cdot \frac{d}{v_{\text{e}}}\right] \tag{3}$$

As outlined above, it is also possible for a single avalanche to induce breakdown by the so-called *streamer mechanism*. When the electron amplification in the gas is sufficiently large (electron number in an avalanche exceeding $n_{e,\text{crit}} = 10^6 \ldots 10^8$), the field associated with the space charge of the avalanche can significantly distort the background field; secondary avalanches can grow in the field-enhanced region and lead to the formation of a *streamer channel*. This channel can further develop into the filamentary breakdown channel known as a *spark*. Several authors have suggested criteria for streamer inceptions of varying complexity. Raether's ignition condition for streamer breakdown requires the ionization integral S to be larger than the logarithm of a critical number $n_{\text{e,crit}}$ of electrons in the avalanche head [16]

$$S = \int_0^d \alpha_{\text{eff}} \cdot \text{dx} = \text{K}_{\text{st}} \stackrel{\text{def}}{=} \ln\left(n_{\text{e,crit}}\right) \tag{4}$$

The *streamer constant* K_{st} can be derived from first principles. For submillimeter gaps and synthetic air, K_{st} varies as a function of gap distance and pressure according to Equation (5) [17]. For the gap distances and pressures considered here, the corresponding range is $\text{K}_{st} \approx 14 \ldots 17$.

$$\text{K}_{st} = \ln\left(\max\left(\frac{7.3710^6}{p/\text{bar}}\right), 1.71 \cdot 10^7 d/\text{mm}\right) \tag{5}$$

Once the streamer channel is formed, its velocity is generally one order of magnitude greater than the electron drift velocity. The formative time is thus approximated as the time an electron avalanche needs to grow to the critical size (Equation (6)) [18].

$$t_{\text{f,s}} = \frac{\text{K}_{\text{st}}}{\alpha\left(\frac{E}{N}\right) v_{\text{e}}\left(\frac{E}{N}\right)} \tag{6}$$

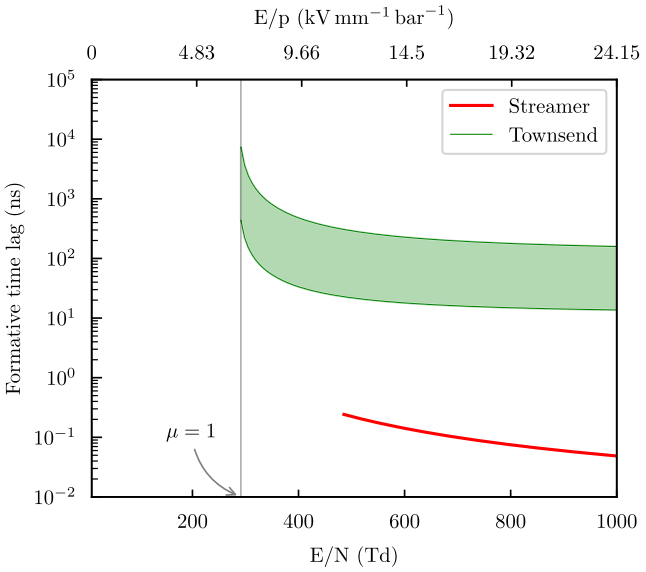

FIGURE 1. Estimated formative times of the streamer and Townsend breakdown mechanisms as a function of the reduced electric field at a 1 mm gap distance (μ is the electron amplification, see Appendix).

The formative times of both mechanisms are compared in Figure 1. The Townsend formative time area is calculated for the range of the relaxation time (τ_1) of the excited species emitting photoelectrons (10-100 ns) and the typical avalanche number E_a of 10^6-10^{10} required to transition into the glow discharge [19].

From criteria (1) and (4), it follows that if $\gamma > n_{e,\text{crit}}^{-1}$, the voltage threshold for a Townsend breakdown is lower than that for streamer inception, and the *static breakdown voltage* V_0 is determined by the Townsend criterion. However, if the voltage increases to a sufficiently large *overvoltage* (see Figure 10 in [17]) during the statistical time lag t_s (i.e., after crossing the Townsend threshold), then the streamer criterion is reached, and a seed electron can induce a streamer breakdown in the first avalanche generation.

2) SEED ELECTRON PROVISION

All breakdown mechanisms start with the appearance of a seed electron, which starts the ionization process that ultimately leads to a breakdown. Seed electrons can originate from the background gas or the cathode surface. The required ionization energy (gas) or work function (cathode) can be provided by a multitude of processes, among which cosmic and radioactive background radiation as well as energetic photons (UV, X-ray, ...) are commonly mentioned [20]. The electric field itself can assist the release of an electron from the cathode in what is called *field emission* or *thermionic*

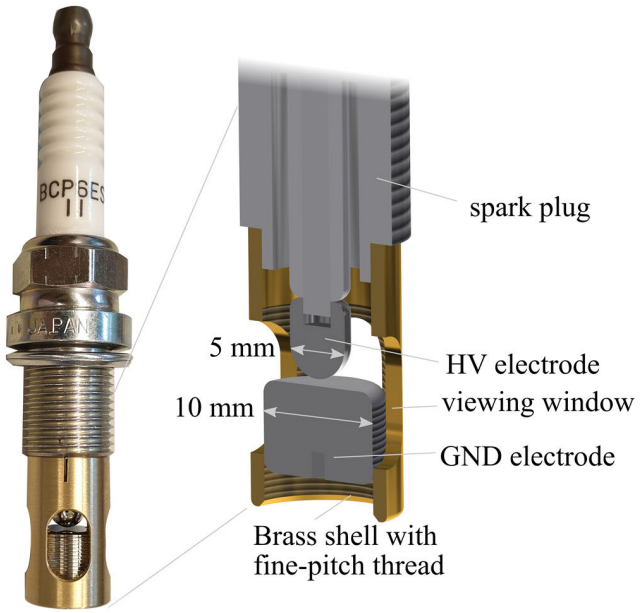

FIGURE 2. Modified sparkplug with hemispherical HV electrode and plane-cylindrical GND electrode.

emission (combined effect of the cathode electric field and temperature) of electrons [21]. Moreover, in *electronegative gases* such as synthetic air, unstable negative ions can constitute an important source of seed electrons [13]. The mentioned processes are subject to statistical fluctuations, which gives rise to a *statistical time lag*, i.e., the time interval between the crossing of the static breakdown threshold and the appearance of the seed electron. The total delay time is the sum of the statistical time lag and the formative time lag:

$$t_{\text{delay}} = t_{\text{s}} + t_{\text{f}}. \tag{7}$$

While the potential sources described above are known, their relative contribution to a given electrode material, gap distance, gas type, and gas pressure often remains unclear.

B. EXPERIMENTAL SETUP

The constant volume cell introduced in [22] is used to characterize the breakdown onset for static and nanosecond pulsed voltages. The absolute pressure in the constant volume cell is varied from 1.5 to 8 bar (six pressure values).

An automotive sparkplug (depicted in Figure 2) is modified to obtain a quasi-uniform electric field between the electrodes.

The *field efficiency factor* [14] decreases with increasing gap size and ranges from 0.98 for the 0.1 mm gap to 0.78 for the 1 mm gap. The cylindrical ground (GND) electrode is held in place by a brass shell. The high-voltage electrode is a half-sphere with a diameter of 5 mm. The distance between the high-voltage (HV) and ground electrodes can be adjusted between 0.1 and 1 mm by means of a fine-pitch thread and precision gauges. From breakdown tests on gaps with the same nominal gap setting, the maximum relative deviation of breakdown voltages due to systematic errors in gap distance is determined to be approximately $\pm 10\%$.

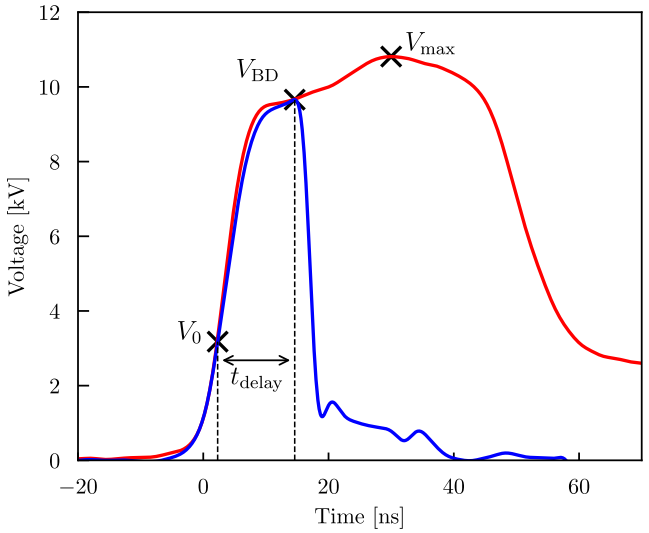

FIGURE 3. Nanosecond voltage pulse prospective voltage (red) and gap voltage (blue) at 1.5 bar and 0.1 mm gap distance with aluminum electrodes.

The first few breakdowns conditioned the electrodes. After the preliminary tests, the electrodes did not show any further "conditioning effect". The static breakdown voltage was measured for different conditions at the start and end of the measuring campaign and did not show any appreciable difference. This suggests that the impact of field distortions caused by the discharge's micro-asperities remained constant throughout the experiments.

A DC high-voltage module capable of generating up to 12 kV is used to perform short-term breakdown tests under slowly increasing voltage. The voltage is monitored with a high-voltage probe (Tektronix p6015a) during the voltage increase (ca. 100 V/s), and the recording is triggered on the breakdown current pulse.

Nanosecond pulses are generated by a commercial nanosecond pulse generator (FID 30-100NM), which has a maximal amplitude of 15 kV into 100 Ω and a pulse duration of 50 ns (FWHM). The typical pulse rise time from 10 to 90% of the maximum is 9 ns, and it has a slight dependence on the maximal pulse amplitude. Figure 3 depicts in red the prospective voltage waveform, i.e. the voltage waveform that would appear across the gap if no breakdown occurred, while in blue the actual gap voltage.

The overvoltage at the time of breakdown is given by the difference between the *dynamic breakdown voltage* $V_{\text{BD}} = V\,(t_{\text{s}} + t_{\text{f}})$ and the *static breakdown voltage* V_0

$$\Delta V_{\text{BD}} = V\,(t_{\text{s}} + t_{\text{f}}) - V_0, \tag{8}$$

The associated *impulse factor* is obtained by normalizing the overvoltage with the static breakdown voltage,

$$K \overset{\text{def}}{=} \frac{\Delta V_{\text{BD}}}{V_0} = \frac{V_{\text{BD}}}{V_0} - 1. \tag{9}$$

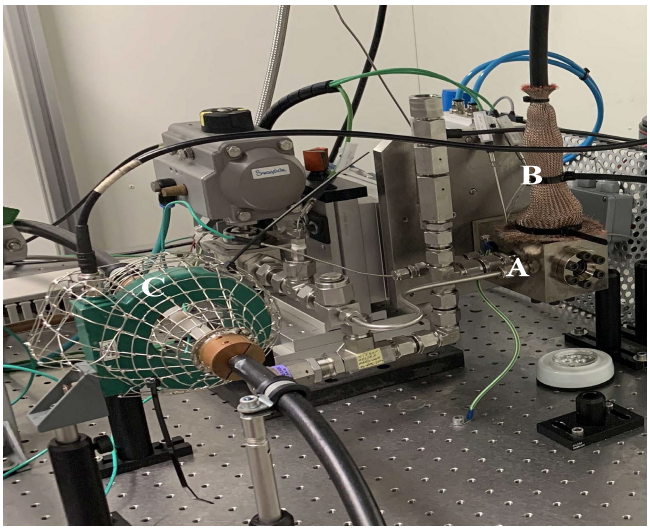

FIGURE 4. Experimental setup: A-constant volume cell, B-coaxial cable shielding, C-current monitor.

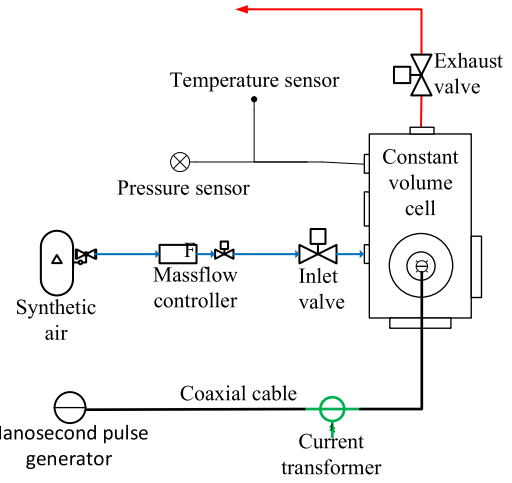

FIGURE 5. Experimental setup: Schematic.

For the classification of the *prospective voltage waveforms*, the *maximal impulse factor* is used,

$$\sigma \stackrel{\text{def}}{=} \frac{V_{\max}}{V_0} - 1, \tag{10}$$

where $V_{\max}$ is the maximum value of the prospective voltage.

The maximal impulse factor, Equation (10), uniquely defines the pulse.

The modified sparkplug is connected to the pulse generator with a 30-m long coaxial cable. Since the pulse propagation time in the cable is longer than the pulse duration, the transmission line wave equation describes the electric circuit active during the discharge. When the high voltage pulse arrives at the anode, it is in part reflected and in part transmitted depending on the ratio between the cable impedance and the output impedance. The voltage and current at the gap are reconstructed by measuring the incident and reflected current waveform inside the coaxial cable. For this reason, a shielded current monitor (Pearson current monitor model 6585 with a usable rise time of 1.5 ns) is placed in the middle of the coaxial cable, where the shield of the cable is removed and reconstructed around the current monitor. The details and validation of the measurement technique are reported in [11].

The HV electrode is connected to the center core of the coaxial cable, while the ground electrode is connected to the coaxial cable's shield through the ignition cell. Figure 4 shows the ignition cell setup.

Figure 5 shows a scheme of the experimental setup. The synthetic air (79.05% nitrogen and 21.05% oxygen) is fed into the constant volume cell via a mass flow controller (Bronkhorst). The ignition cell is equipped with pneumatically actuated in- and outlet valves.

Positive polarity pulses are used in this investigation; therefore, the HV electrode is positive (anode), while the ground electrode is negative (cathode). A more detailed description of the system's setup, and electrical characterization can be found in [11].

C. UV ILLUMINATION

A mercury lamp is mounted onto the fused silica glass window of the constant volume cell to illuminate the cathode with UV light in selected experiments. The impact of UV illumination is tested in both the static and nanosecond pulsed cases.

D. MATERIAL EFFECT

Electrodes (HV and GND) made of aluminum, copper, and stainless steel are used to investigate the impact of the electrode material on the breakdown voltage in both the static and pulsed voltage cases. The effect on breakdown time lag is also quantified for the pulsed voltage. The materials were chosen because of their difference in the vacuum work functions, which are ∼4.26 eV (Al), ∼4.47 eV (Cu), and ∼5.08 eV (Steel), respectively [23], [24].

E. ELECTRIC FIELD DATA

The electric field is determined with COMSOL Multiphysics software. The electrode system is modeled with rotational symmetry, as shown in Figure 6, based on the geometry shown in Figure 2. Only the electric field lines ending on the GND electrode are considered in this analysis. The field amplitude is shown for a voltage of 1 V and is scaled accordingly for the actual applied voltages.

III. RESULTS

A. STATIC BREAKDOWN VOLTAGE

Figure 7 shows the breakdown voltage value under a slowly increasing voltage (∼0.1 kV/s) for ambient temperature and absolute pressures ranging from 1.5 to 8 bar. The gap size is varied, where possible, from 0.1 mm to 1 mm. The full line for the 3-bar case represents the breakdown values according to Townsend theory for $\gamma = 2.2 \cdot 10^{-4}$. The minimum and

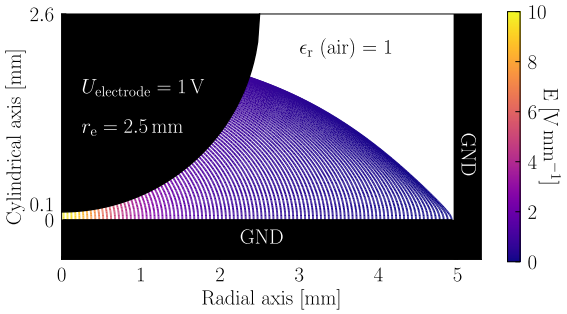

FIGURE 6. Electric field simulation for a gap distance of 0.1 mm.

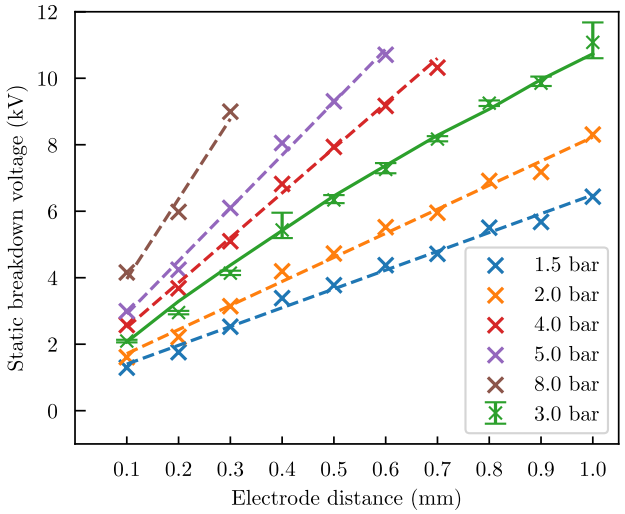

FIGURE 7. Static breakdown voltages as a function of gap distance and synthetic air pressure (for steel electrodes).

maximum measured breakdown values are shown as well for the 3-bar case. The dashed lines represent a linear fit of the calculated mean breakdown value for a given pressure.

A linear fit follows Townsend theory in the investigated pressures and gap sizes. The indicated measured values are averaged over approximately 20 breakdown measurements. The maximal relative deviation of individual readings from the mean value is always below 10% for each experiment, while the average of the maximal deviations for all the investigated conditions is ∼3%. The relative deviation of the mean value with respect to the fit line remains below ∼12%, with an average deviation of ∼3%. Figure 7 shows that the mean breakdown voltage increases approximately linearly with gap distance.

Figure 8 illustrates the effect of UV illumination on the static breakdown voltage. The box plot represents, from top to bottom, the maximal measured value, the 75th percentile, the mean value, the 25th percentile, and the minimal value. The mean breakdown voltage under UV illumination is lower in the investigated cases. No relative error in gap distance is present because the electrode distance is not reset between the experiments with and without UV illumination. Generally, the relative lowering of mean breakdown voltages is more significant at lower pressure-gap distances, as is the

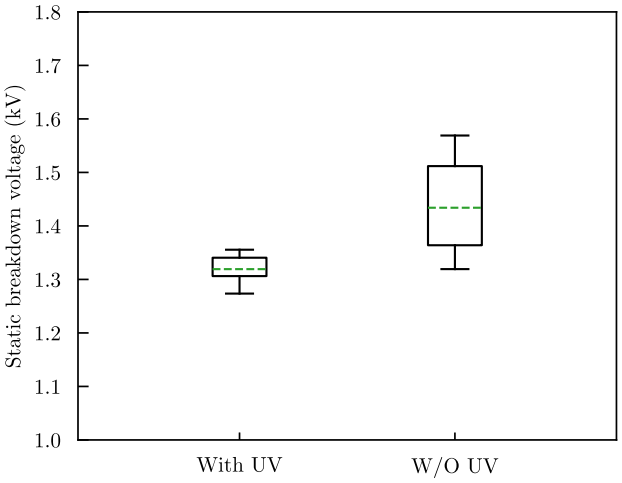

FIGURE 8. UV impact on the static breakdown voltage at 1.5 bar and 0.1 mm gap distances with steel electrodes.

TABLE 1. UV impact on the static breakdown voltage.

Condition (p,d)	Mean (w/o UV)	Mean (UV)	p value
1.5 bar, 0.1 mm	1.43 kV	1.32 kV	4.6×10^{-7}
3 bar, 0.5 mm	6.11 kV	6.02 kV	2.5×10^{-4}
3 bar, 0.9 mm	9.44 kV	9.35 kV	9.8×10^{-4}

reduction in scattering around the mean. An overview of the results is given in Table 1. Breakdown voltages and times are subject to relatively large scatter even when all experimental parameters are held constant. Therefore, the *Mann-Whitney* U test is used, whose *p value* indicates the probability that the measured variation is just due to the finite sample size (see appendinx B). For example, the probability that the observed differences between the sample with and without UV illumination at 1.5 bar and 0.1 mm is pure chance is less than$\cdot 10^{-6}$.

Table 2 lists an example measurement of the static breakdown voltage for the three different materials, a gap size of 0.5 mm and a pressure of 1.5 bar. The p value is the result of the *Mann–Whitney U test* between the two different sets of results for the two materials in parentheses. The measured mean breakdown voltages are on the order of the associated cathode vacuum work functions. To take into account the effect of the gap size error, the breakdown voltages of each material were measured three times consecutively by resetting the electrode distance to the same nominal gap distance. When the associated sample's breakdown voltage means did not show a significant difference ($p > 0.05$), i.e., hen the distance setting did not significantly change the observed breakdown values (as is the case reported in Table 2), ordering according to the work function values was observed. In some instances, however, the error introduced by the gap setting dominated the order of the mean breakdown values. In these cases, it could be seen that the mean breakdown values of

TABLE 2. Electrode material impact on the static breakdown voltage.

Material	Mean Voltage	95% Confidence interval	p value
Steel	3.73 kV	0.024 kV	0.01 (Steel- Cu)
Copper	3.65 kV	0.044 kV	1.96×10^{-6} (Cu-Al)
Aluminum	3.51 kV	0.048 kV	1.85×10^{-12} (Al -Steel)

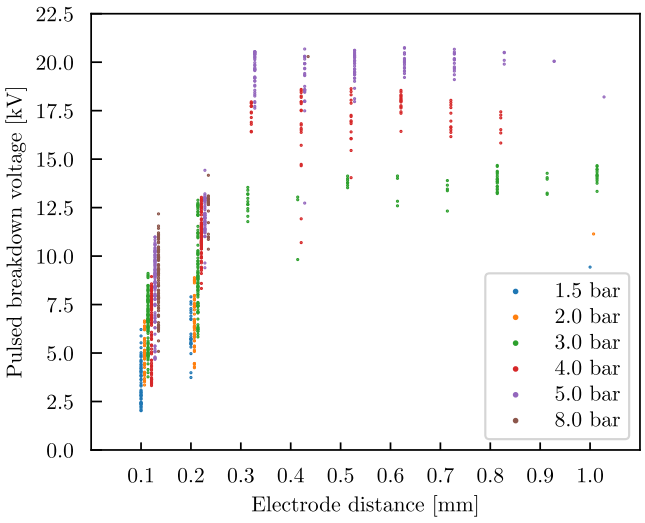

FIGURE 9. Pulsed breakdown voltages as a function of gap distance and synthetic air pressure (for steel electrodes).

the three repetitions indeed showed a significant difference ($p < 0.05$).

B. PULSED BREAKDOWN VOLTAGES AND BREAKDOWN TIMES

Figure 9 and Figure 10 shows respectively the breakdown voltage and breakdown time of 1093 experiments with pulsed voltages in synthetic air with pressures ranging from 1.5 to 8 bar and for electrode distances between 0.1 and 1 mm in 0.1mm steps.

For clarity reasons, the breakdown voltages and times are slightly offset to the right for increasing pressures.

As shown in Figure 1, the formative time lag is negligible compared to the measured delay times. The statistical time lag t_s causes a breakdown to occur at a certain overvoltage characterized by the impulse factor K (Equation (9)). The measured impulse factors ranged from 0.2 to 4.4 for the different conditions and were above the corresponding Townsend-to-streamer transition voltages for $\gamma = 2.2 \cdot 10^{-4}$ (see Section II.I.1 and references therein). Due to the short but non-negligible pulse voltage rise time of approximately 9 ns, breakdown can occur on the rising part of the pulse as well on the nearly flat part of the pulse. The maximal impulse factor σ describes where the breakdown occurs.

Figure 11 and Figure 12 provides respectively an overview of the measured impulse factors and the measured breakdown

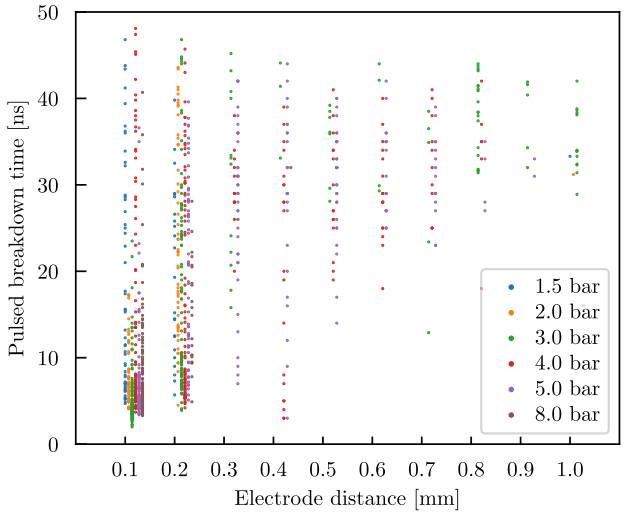

FIGURE 10. Delay time under pulsed breakdown voltages as a function of gap distance and synthetic air pressure (for steel electrodes).

time for a 0.1 mm gap at 1.5 bar pressure and ambient temperature under 52 voltage pulses of different maximal impulse factors. The box plots in Figure 11 and Figure 12 represent from top to bottom the maximal measured value, the 75% percentile, the mean value, the 25% percentile, and the minimal value. Breakdown occurs with relatively small scatter near the voltage maximum for maximal impulse factors $\sigma < 2$ (rising line). At higher prospective overvoltages, the achieved impulse factors are considerably smaller than the maximal impulse factor, indicating that breakdown occurs in the early rising part of the pulse. In addition, the scatter in the breakdown voltages is significantly larger.

The measured breakdown times follow a specific pattern. As shown in Figure 12, they fall off rapidly with increasing maximum overvoltage of the applied pulse ($0.5 < \sigma < 2$) but show a saturation for $\sigma > 2$. For the breakdown times, the scatter decreases with increasing overvoltage.

Only one experimental point is present for ($\sigma = 5.5$), represented by the green line, since the calculation of percentiles, minimal, and maximal values is impossible.

These trends of breakdown voltages and times are present at different pressures and gap distances whenever high maximal impulse factors are reachable with the setup used.

Figure 13 shows the impact of UV illumination on breakdown times for the 0.1 mm gap size and 8 bar synthetic air pressure. The mean value and the 95% confidence interval of the mean are reported in the plot. The shown result is representative of all the investigated conditions where the range of accessible σ was large. The mean breakdown times and their scatter are significantly lower in the presence of UV light, but the effect decreases with increasing overvoltage.

The effect of different materials on the mean breakdown threshold under pulsed voltages is illustrated in Figure 14 for a 0.2 mm gap size, synthetic air pressure of 3 bar, and ambient temperature. The mean value and the 95% confidence interval of the mean are reported. Interestingly, the steel electrodes

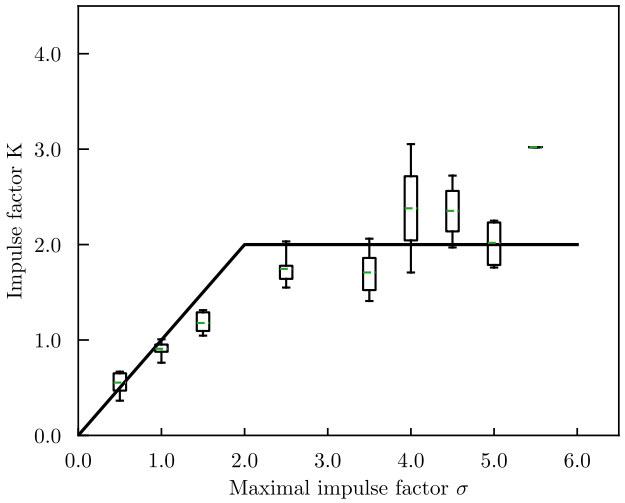

FIGURE 11. Measured impulse factors (relative overvoltage at breakdown) as a function of the maximal impulse factor (maximum relative overvoltage of the applied pulse) at 1.5 bar and 0.1 mm.

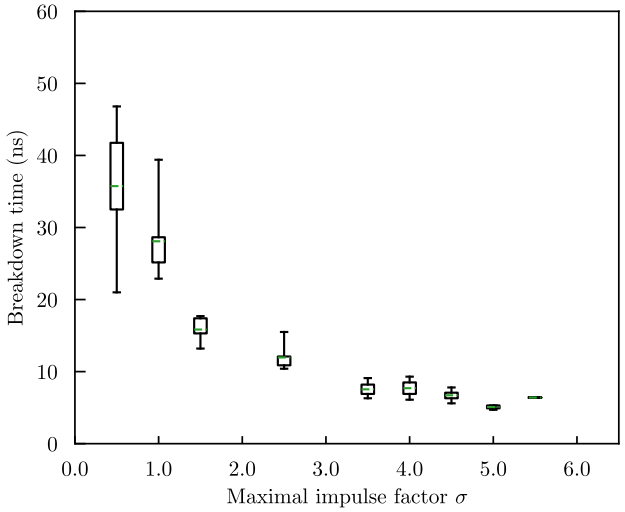

FIGURE 12. Measured breakdown time as a function of the maximal impulse factor at 1.5 bar and 0.1 mm gap distance.

show a significantly higher breakdown threshold than the aluminum and copper, and there is even a significant fraction of cases (∼15%) where no breakdown occurred with the steel electrodes for the tested range of overvoltages. To check the validity of the experimental results, the measurement series was repeated for the steel electrodes (rep#2), and the previously obtained values (rep#1) were confirmed. Moreover, a possible bias due to fluctuations in the maximum prospective pulse voltage was examined: it turned out that the prospective pulse amplitudes applied to the steel electrodes were even slightly larger (see Figure 14, top) and cannot explain the significantly larger breakdown values. The maximum prospective voltage is between 10.5 and 11.5 kV. The horizontal line in Figure 14 represents the static breakdown voltage for the shown condition.

Figure 15 depicts the mean breakdown time and the 95% confidence intervals of the experiments where a breakdown

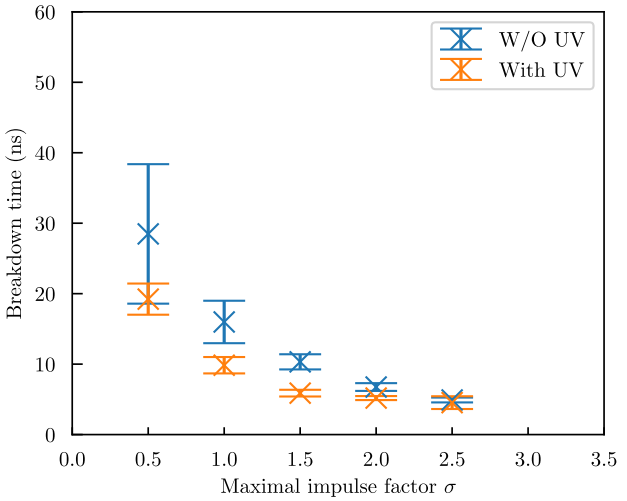

FIGURE 13. Impact of UV illumination on the breakdown time as a function of the maximal impulse factor.

was detected. The m and n numbers on the top of Figure 15 lists the number of experiments with and without breakdown, respectively.

C. BREAKDOWN TIME ANALYSIS: SEED ELECTRON GENERATION RATE

This section aims to derive an expression for the seed electron generation rate as a function of the gap electric field strength. The following analysis is meant to provide an order of magnitude estimation, thus including a number of simplifying steps. For example, due to the quasi-uniform geometry, a mean electric field strength U/d is attributed to the applied voltage U and used to parametrize the derived electric field dependencies. The analysis is carried out for 0.1 mm and 0.2 mm gap distances and pressures of 1.5, 2, 3, 4, 5, and 8 bar, as these conditions fully cover the experimentally accessible range of electric fields up to approximately 120 kV/mm. A total of 960 breakdown measurements are available for the analysis.

An important parameter in the analysis is the *active cathode area* A_{act}, which is the area on the cathode where the associated field lines satisfy the streamer criterion (5) for $K_{st} > 16$. Thus, a free electron near the active cathode area is likely to induce a breakdown, while outside this area, it is likely to become attached and simply drift to the anode. The attachment and ionization coefficients required for this calculation are extracted from the Boltzmann equation solver BOLSIG+ [25] using the cross-sectional datasets reported in [26]–[28].

First, the dependence of the average time to breakdown on the electric field strength is derived from the measurement data in the following way. A list of voltages with equally spaced bins spanning a range from the calculated streamer onset voltage to the largest measured breakdown voltage is defined for each pressure and gap distance. The voltage list size is chosen so that the distance between the values is ca. 500 V. Division by the gap distance generates an associated (mean) electric field list $[E_i]$. Let then Δt_i be the cumulated

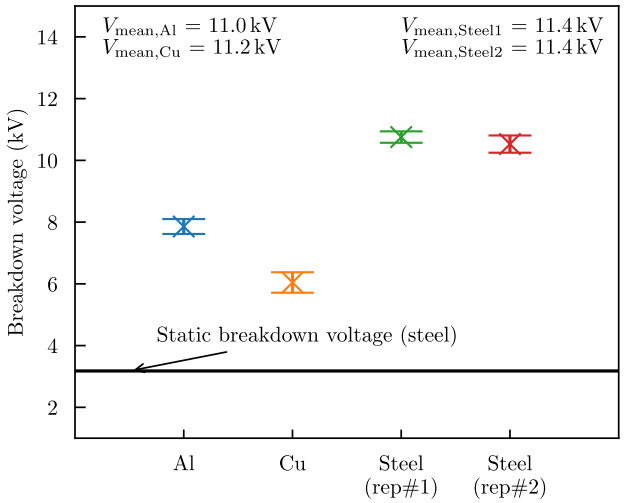

FIGURE 14. Electrode material effect on the breakdown voltage under pulsed voltages at 3 bar and 0.2 mm gap distance.

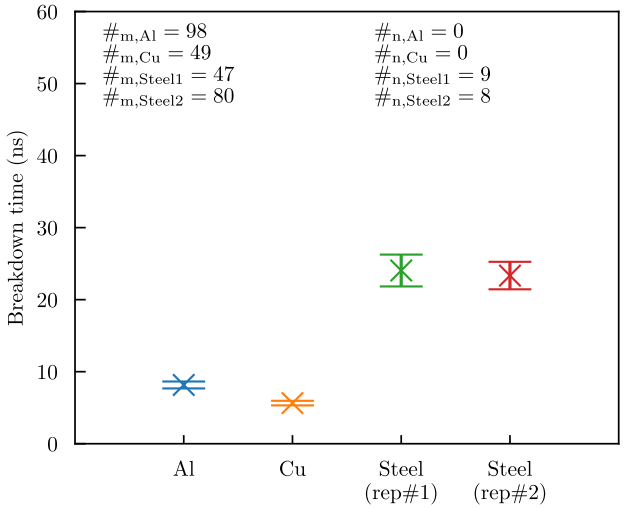

FIGURE 15. Electrode material effect on the breakdown times under pulsed voltages at 3 bar and 0.2 mm gap distance.

time (i.e., from all measurements at a given pressure and gap distance), let the applied mean electric field $U(t)/d$ value lie in bin number i, and let O_i be the number of observed breakdown values in this bin. The average time the system gas is "stable" (no breakdown) when exposed to the field E_i is given by

$$t_{BD}(E_i) = \frac{\Delta t_i}{O_i}. \tag{11}$$

This average time to breakdown is shown in Figure 16 for gap distances of 0.1 mm and 0.2 mm and all available pressures. The time to breakdown is determined by the number of electrons generated near the *active* cathode area per unit time. Thus, if $\dot{n}_e(E)$ is the seed electron generation per unit time and cathode area at the electric field strength E, then

$$t_{BD}(E) \approx t_s(E) = \frac{1}{A_{act}(E) \cdot \dot{n}_e(E)}. \tag{12}$$

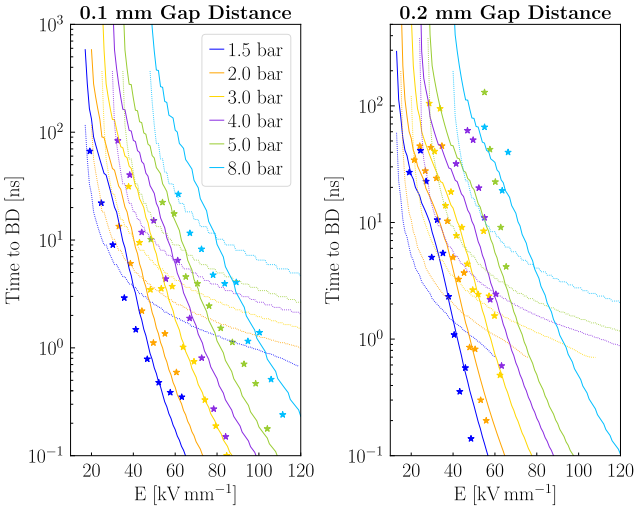

FIGURE 16. Determined mean times to breakdown as a function of the gap electric field. Fit lines are based on seed electron generation rates with (full line) and without (dotted line) activated field emission.

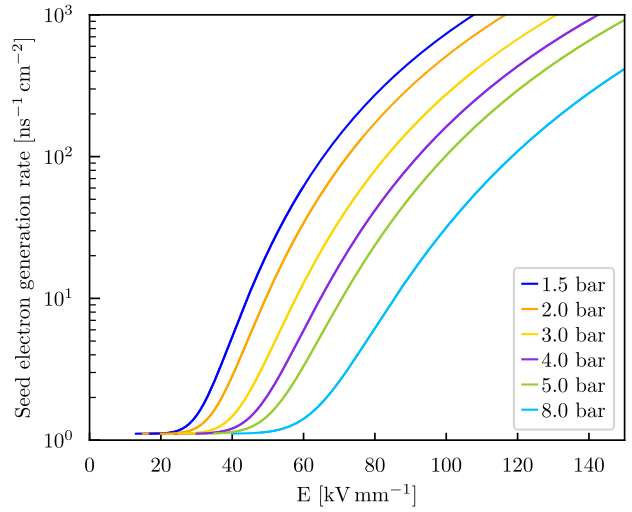

FIGURE 17. Derived seed electron generation rate as a function of the electric field.

The only unknown quantity is then $\dot{n}_e(E)$. Note that the formative time is negligible with respect to the measured time to breakdown and can thus be omitted in Equation (12). The dotted lines in Figure 16 indicate that field-independent seed electron generation does not fit the experimental data adequately. Instead, the full lines are based on a field emission contribution based on the Fowler–Nordheim formula [29] (with empirically derived parameters), which is activated at high fields on top of a constant background rate $\dot{n}_{e,0}$,

$$t_{BD}(E) = \frac{1}{A_{act} \cdot \left[\dot{n}_{e,0} + C \cdot E^2 \cdot \exp\left(-\frac{Dp^b}{E}\right)\right]}. \tag{13}$$

A least-square fit over the 112 available data points for 0.1 mm and 0.2 mm gap distances leads to the following parameters: $\dot{n}_{e,0} = 1.1$ ns^{-1} cm^{-2}, $C = 6.7{\cdot}10^3$ ns^{-1}kV^{-2}mm^2, $D = 178$ kV mm^{-1} and the coefficient $b = 0.53$.

Figure 17 shows the resulting seed electron generation as a function of the mean gap electric field.

IV. DISCUSSION

The observed quasi-linear increase in the static breakdown voltage with the gap distance is in good agreement with the predictions from Townsend's theory and a secondary feedback emission coefficient of $\gamma = 2.2 \cdot 10^{-4}$, which is a typical value reported for air [30]. Indeed, all the investigated cases are well above the Paschen minimum at $(p \cdot d)_{\min} = 7.3\ \mu\text{m} \cdot \text{bar}$ [14], which explains the approximately linear increase with both pressure and gap distance.

The reduction of the statistical spread in the static breakdown voltage under UV illumination might, on a first account, be attributed to the corresponding increase in seed electron generation. UV illumination reduces the statistical time lag and hence the breakdown voltage (dU/dt is small but not zero). However, with a background rate of $\dot{n}_{\text{e,bk}} = 1.1\ \text{ns}^{-1}\ \text{cm}^{-2}$, the voltage slew rate would need to be much larger than the applied ∼100 V/s to see any observable spread in the breakdown voltage. A possible explanation is the following. Just around the onset voltage of Townsend breakdown, the active area is concentrated to a small section at the tip of the half-sphere. The probability of a seed electron triggering a sequence of avalanches, in which all feedback photons hit the active area, can be exceedingly small. This means that the vast majority of secondary seed electrons will not induce breakdown, and hence, the apparent statistical time lag is much larger than what is expected from the seed electron generation rate. This reasoning assumes that the main secondary feedback mechanism is the photoeffect at the cathode, which is in accordance with the available literature for pressurized air and metallic electrodes [20].

The simultaneously observed lowering of the average static breakdown voltage under UV illumination is also in line with qualitative theoretical reasoning based on the increase in the amplification factor $\mu' > \mu$ in the presence of a constant source of external seed electrons [19].

Finally, the reduction of the static breakdown voltage with the reduced cathode work function values can also be explained within Townsend's theory by an increase in the amplification factor (larger secondary electron emission coefficient). All observations support the conclusion that the discharge under slowly increasing voltages and the investigated range of *pd* values from 0.1 to 8 mm·bar is governed by the Townsend mechanism.

The remainder of the discussion is dedicated to breakdown under nanosecond pulsed voltages, for which the DC breakdown voltages serve as a helpful point of reference. Due to the short rise time of the voltage pulse (∼9 ns), large overvoltages can develop during the time before a seed electron appears. Indeed, breakdown voltages exceeding the static threshold by up to 440% were observed.

Two breakdown regimes are present (see Figure 11 and Figure 12): at a low maximal impulse factor, the breakdown time has large variability, but the breakdown voltage has low scatter. Conversely, at high maximal impulse factors, the breakdown voltage scatters significantly, whereas the time falls in a relatively narrow interval. Similar breakdown regimes are reported in [11]; where, due to the complex geometry involved, the calculation of the active area was not possible.This behavior can be related to the employed voltage pulse shape. When the maximum overvoltage is small, breakdown is likely to occur in the plateau of the pulse because seed electrons are unlikely to become available in the few nanoseconds it takes to reach the voltage plateau in the small active area that is created by the low overvoltages. The breakdown voltage is equal to the plateau voltage, and breakdown times span the whole duration of the pulse (up to 50 ns). In contrast, when the maximum overvoltage is large, seed electrons are generated at a higher rate over a larger area due to the large fields developing during the rising edge of the pulse or shortly thereafter. With the breakdown occurring in this interval, the breakdown times are small and localized, whereas the breakdown voltages scatter significantly due to the large dU/dt (even minor breakdown time variations result in significant breakdown voltages variation). For a synthetic air gap of 0.1 mm and pressure of 1.5 bar, the breakdown times for impulse factors above 3 vary between 5and 9 ns, with the latter being equal to the typical pulse rise time.

The sharp transition between the two regimes also supports the conclusion of a field-dependent seed electron generation rate. Without the field emission, the breakdown rate increase should follow the slower increase in the active area.

The quantitative analysis presented in Section III.III shows that the time to breakdown is a strongly decreasing function of the electric field. For relatively small field strengths, the increase in the active area can explain the observed decrease in the mean breakdown time. However, this effect alone cannot explain the rate of decrease of breakdown times at higher field strengths, where the seed electron generation rate itself seems to increase significantly above the low-field (background) value. The measured breakdown times are well reproduced by a Fowler-Nordheim-type equation [29], suggesting a field emission of electrons from the cathode. The proposed parameterization of the associated seed electron generation represents a novel contribution.

After the field emission activation, electron emissions over the macroscopic surface of $\sim 10^8$ electrons per second and cm^2 are estimated. The release of electrons from cold, heavily oxidized steel electrodes in the atmosphere was reported in [31]. Up to 106 electrons per second were released under an applied field of 1 kV/mm, which matched the prediction based on the Fowle–Nordheim emission equation. The researcher estimated an area from which the electrons are emitted of $\sim 10^{-14}\ \text{cm}^2$, suggesting that the electrons might be liberated from groups of negative ions at the cathode surface.

Comparing the experimentally derived field-dependent seed electron emission rate with the quantitative predictions from the Fowler–Nordheim equation allows the determination of the actively emitting surface fraction and

the effective work function of these emitters as a function of pressure [32]. A pressure-independent active surface fraction of $2{\cdot}10^{-15}$ is obtained, and the effective work function is found to increase from 2.25 eV at 1.5 bar to 4 eV at 8 bar. These numbers suggest that field emission occurs over groups of atoms with low effective work functions. Moreover, a higher gas number density seems to hinder electron emission from these sites. The increasingly effective work function of the emission sites at larger pressure may thus be an effect of adsorption of gaseous constituents onto the emission sites, thereby reducing the electron emission yield.

While the field emission hypothesis paints a consistent picture with the obtained data and has also been previously invoked for the explanation of time lags of electrical breakdown under pressurized gases [34], another a priori plausible explanation (for pulsed breakdown) based on the field-dependent detachment of electrons from unstable negative oxygen ions is argued to be less consistent with the observed data. First, the detachment of electrons occurs on average in a few collisions at fields as low as 3.8 kV mm^{-1} in air at atmospheric pressure [33]. Hence, a negative ion available in the gap before the voltage pulse arrives would lose its electron in a fraction of a nanosecond and not lead to a field-dependent detachment that could explain the observed time delays. Second, if detachment from negative ions would dominate, the detected breakdown dependency on the electrode material should be lower. Third, and even more importantly, the equilibrium number density of unstable negative ions (N_i) is low in the considered small gaps, such that the probability of finding a suitably placed negative ion upon arrival of the voltage pulse is negligible for practical purposes. The maximum equilibrium number density in the gap is proportional to the background ionization rate Q ($\sim$10 cm^{-3} s^{-1}), gap distance d, diffusion coefficient D_i ($5{\cdot}10^{-2}$ cm^2 s^{-1} at 1 bar) and pressure [33]:

$$N_\mathrm{i} = \frac{Qd^2p}{8 \cdot D_\mathrm{i}}. \tag{14}$$

For the $d = 0.2$ mm gap and a pressure of $p = 8$ bar, $N_\mathrm{i} \sim 8{\cdot}10^{-2}$ cm^{-3}, while the active volume is only a fraction of a cm^3. The generation of a seed electron by detachment from negative ions thus seems unlikely in such small gaps, unless the volume ionization rate is increased significantly (e.g., by exposing the gap to artificial ionizing radiation) or nonequilibrium conditions apply (e.g., in repetitively pulsed discharges). It thus remains unclear what is the source of seed electrons constituting the background rate, and more targeted investigations at lower overvoltages are needed to clarify this point.

UV illumination under pulsed voltages is found to increase the background seed electron generation rate approximately fivefold. As expected, this enhancement becomes negligible above the onset field strength for field emission.

The investigation with different electrode materials and pulsed voltages suggests that the field electron emission is affected by the material of the electrodes. Breakdown is observed to occur at the plateau for the steel electrode. Most notably, not all applied pulses with steel electrodes result in a breakdown. Breakdown occurs during the rising part of the applied voltage for the copper and aluminum electrodes. All the experiments result in a breakdown for the copper and aluminum electrodes. This suggests the conclusion that steel has a significantly lower field-enhanced seed electron emission rate than copper and aluminum, which is in accordance with their vacuum work function values. Based on this argument, one would, however, also expect that the seed electron generation rate is the lowest for aluminum electrodes. Nevertheless, the lowest breakdown voltages and times were obtained for the copper electrode. Although the measured prospective voltages were slightly higher in the case of the copper electrodes (see Figure 14), the difference cannot explain the measured trend. One plausible conclusion at present is to envisage that tabulated vacuum work functions may not in all cases be representative of electrodes in pressurized synthetic air. Another explanation could be hidden in the presence of the microstructure on the surface of the electrodes.

Interestingly, similar marked differences between the breakdown strength of pressurized synthetic air for aluminum and steel electrodes under DC voltages and quasi-uniform fields above $\sim$10 kV/mm have been reported in a previous study [34]. The deviation from Paschen's law at high pressures (above $\sim$7 bar) is attributed to the field-assisted electron emission from the cathode surface, which assists the Townsend mechanism, particularly when the macroscopic electric field is on the order of $\sim$50 kV/mm [31], [34]. This is in good agreement with the present results, where strong electric fields are obtained by fast pulse rise times instead of very large pressures. Indeed, depending on the pressure value, a significant reduction in the statistical time lag is observed above $\sim$20 to 60 kV mm^{-1}.

V. CONCLUSION

The breakdowns under slowly increasing and nanosecond pulsed voltages are investigated in pressurized synthetic air (1.5 to 8 bar) in quasi-uniform electric fields with gaps ranging from 0.1 to 1 mm. The main findings are listed below.

- In the investigated conditions under slowly varied voltages, breakdown occurs according to the Townsend mechanism with a secondary feedback emission coefficient of $\gamma = 2.2 \cdot 10^{-4}$.
- The DC breakdown voltage reduction with different electrode materials is in qualitative agreement with the value of the cathode work functions.
- UV light reduces the mean breakdown and the scatter around the mean for DC voltages.
- Compared to the DC case, higher breakdown voltages (up to 440%) are recorded when nanosecond voltage pulses are used.
- The breakdown under nanosecond voltage pulses is affected by UV light. For similarly applied nanosecond voltage pulses, the time to breakdown is on average

shorter and scatters less when UV light is used. The effect vanishes at large overvoltages.
- The breakdown under nanosecond pulsed voltages is affected by the electrode material. Notable differences in the breakdown time and voltage are measured between aluminum/copper and steel electrodes. An analogical breakdown onset could be expected for metals having similar work functions. For example, nickel, which is a typically used material for sparkplugs, has a work function similar to that of steel [35].
- The observed characteristics under nanosecond pulsed voltages are hypothesized to be attributable to an altered seed electron generation mechanism. A constant background emission rate (which can be increased using UV light) is observed at low electric fields. Above a pressure-dependent onset field, most electrons are generated by field emission.
- An expression for the seed electron generation rate consisting of a constant background term and a field emission contribution based on the Fowler–Nordheim formula is derived from the measured breakdown delays under nanosecond pulsed voltages.

APPENDIX

A. FORMATIVE TIME FOR TOWNSEND BREAKDOWN

The formative time of Townsend breakdown is estimated as the time it takes for a certain large number $E_a \sim 10^6 \ldots 10^{10}$ of avalanches to form, which requires an average number r of generations [15] given by:

$$r = \frac{\ln\left[(\mu - 1)\, E_a\right]}{\ln \mu}. \tag{15}$$

The formative time of Townsend breakdown is calculated as the product of the number of generations r and the mean time $\tau_{\mathrm{s.a.}}$ between successor avalanches according to Equation (16). Note that only secondary emission due to the photoelectric effect is considered here, as it is the only mechanism fast enough to be of potential relevance for highly transient voltages.

$$t_{\mathrm{f,T}} = r \cdot \tau_{\mathrm{s.a.}} = \frac{\ln\left[(\mu-1)\, E_a\right]}{\ln \mu} \cdot \left[\tau_1 + \left(1 - \frac{1}{\alpha_{\mathrm{eff}} \cdot d}\right) \cdot \frac{d}{v_{\mathrm{e}}}\right] \tag{16}$$

τ_1 is the deexcitation time of the species emitting the feedback photons. The photons are mostly emitted close to the anode, especially at high electron amplification, which is considered by the factor $1 - (\alpha_{\mathrm{eff}} \cdot d)^{-1}$.

B. TEST FOR STATISTICAL SIGNIFICANCE (P VALUE)

Breakdown voltages and times are subject to relatively large scatter even when all macroscopic parameters are held constant. It is thus often not directly obvious from the measured data whether a change in the experimental conditions indeed influences the underlying probability distribution (i.e., the breakdown process). The difference in the collected data may be due to random variations that occur in finite sample sizes. In such cases, statistical tests are required, which determine (under certain assumptions) the probability that the observed difference in, e.g., the mean breakdown voltage, is just due to the finite sample size. In this paper, the *Mann–Whitney U test* [36] is used, whose *p value* indicates the probability mentioned above that the null hypothesis H_0 = "the underlying probability distributions are the same" is true. For example, $p = 0.01$ means that in 1 out of 100 experiments, one would expect to find the observed difference just by chance. The Mann–Whitney U test is nonparametric and, in particular, does not assume normality of the underlying distributions. This comes at the cost of lower power, i.e., a larger probability of a Type II error (not rejecting H_0 when it is false).

ACKNOWLEDGMENT

(Raphael Färber, Yang Lu, and Michelangelo Balmelli contributed equally to this work). The authors would like to thank Ondrej Sefl for the thorough revision of the manuscript, also would like to thank Hugo Ehrensperger, Roland Graf, Thomas Hilfiker, and Roland Spühler for their precious help in the experimental test bench setup, and also would like to thank the ABB Switzerland for borrowing the pulse generators used for this analysis.

REFERENCES

[1] D. H. Lee, "Hydrogen production via the Kværner process and plasma reforming," in *Compendium Hydrogen Energy*. Amsterdam, The Netherlands: Elsevier, 2015, pp. 349–391, doi: 10.1016/B978-1-78242-361-4.00012-1.

[2] W. Eckstein, "Sputtering yields," in *Sputtering by Particle Bombardment*, vol. 110. Berlin, Germany: Springer, 2007, pp. 33–187, doi: 10.1007/978-3-540-44502-9_3.

[3] J. C. Hilliard and G. S. Springer, *Fuel Economy*. Boston, MA, USA: Springer, 1984, doi: 10.1007/978-1-4899-2277-9.

[4] R. Färber, T. Guillod, F. Krismer, J. Kolar, and C. Franck, "Endurance of polymeric insulation foil exposed to DC-biased medium-frequency rectangular pulse voltage stress," *Energies*, vol. 13, no. 1, p. 13, Dec. 2019, doi: 10.3390/en13010013.

[5] J. B. Heywood, *Internal Combustion Engine Fundamentals*. New York, NY, USA: McGraw-Hill, 1988.

[6] S. V. Pancheshnyi, D. A. Lacoste, A. Bourdon, and C. O. Laux, "Ignition of propane—Air mixtures by a repetitively pulsed nanosecond discharge," *IEEE Trans. Plasma Sci.*, vol. 34, no. 6, pp. 2478–2487, Dec. 2006, doi: 10.1109/TPS.2006.876421.

[7] W. Vera-Tudela, L. Merotto, M. Balmelli, and P. Soltic, "Experimental study of the ignition of lean methane/air mixtures using inductive and NRPD ignition systems in the pre-chamber and turbulent jet ignition in the main chamber," *Energy Convers. Manage.*, vol. 252, Jan. 2022, Art. no. 115012, doi: 10.1016/j.enconman.2021.115012.

[8] L. Merotto, M. Balmelli, W. Vera-Tudela, and P. Soltic, "Comparison of ignition and early flame propagation in methane/air mixtures using nanosecond repetitively pulsed discharge and inductive ignition in a pre-chamber setup under engine relevant conditions," *Combustion Flame*, vol. 237, Mar. 2022, Art. no. 111851.

[9] V. Gururajan, R. Scarcelli, S. Biswas, and I. Ekoto, "CFD modeling of low temperature ignition processes from a nanosecond pulsed discharge at quiescent conditions," in *Proc. ASME Internal Combustion Engine Division Fall Tech. Conf.*, Oct. 2021, Art. no. V001T06A010, doi: 10.1115/ICEF2021-67902.

[10] V. Gururajan and R. Scarcelli, "A nanosecond pulsed discharge circuit model for engine applications," *J. Phys. D, Appl. Phys.*, vol. 55, no. 15, Apr. 2022, Art. no. 155205, doi: 10.1088/1361-6463/ac4726.

[11] M. Balmelli, R. Farber, L. Merotto, P. Soltic, D. Bleiner, C. M. Franck, and J. Biela, "Experimental analysis of breakdown with nanosecond pulses for spark-ignition engines," *IEEE Access*, vol. 9, pp. 100050–100062, 2021, doi: 10.1109/ACCESS.2021.3095664.

[12] N. Hayakawa, F. Shimizu, and H. Okubo, "Estimation of partial discharge inception voltage of magnet wires under inverter surge voltage by volume-time theory," *IEEE Trans. Dielectr. Electr. Insul.*, vol. 19, no. 2, pp. 550–557, Apr. 2012, doi: 10.1109/TDEI.2012.6180249.
[13] X. Xu, S. Jayaram, and S. A. Boggs, "Prediction of breakdown in SF_6 under impulse conditions," *IEEE Trans. Dielectr. Electr. Insul.*, vol. 3, no. 6, pp. 836–842, Dec. 1996, doi: 10.1109/94.556569.
[14] A. Küchler, *High Voltage Engineering*. Berlin, Germany: Springer, 2018, doi: 10.1007/978-3-642-11993-4.
[15] W. Legler, "Zur statistik der elektronenlawinen," *Zeitschrift Physik*, vol. 140, no. 2, pp. 221–240, Mar. 1955, doi: 10.1007/BF01349380.
[16] H. Raether, *Electron Avalanches and Breakdown in Gases*. Dc, Usa, Washington: Butterworths, 1964. [Online]. Available: https://books.google.ch/books?id=2nSCvEq6AFcC
[17] R. Färber and C. M. Franck, "Streamer inception thresholds derived from a statistical electron transport model," *J. Phys. D, Appl. Phys.*, vol. 54, no. 43, Oct. 2021, Art. no. 435202, doi: 10.1088/1361-6463/ac1888.
[18] G. A. Mesiats, *Pulsed Power*. New York, NY, USA: Kluwer, 2005.
[19] N. A. Kapcov. (1955). *Elektrische Vorgänge in Gasen und im Vakuum. Deutscher Verlag der Wissenschaften*. [Online]. Available: https://books.google.ch/books?id=3io6AQAAIAAJ
[20] M. Beyer, W. Boeck, K. Müller, and W. Zaengl, *Hochspannungstechnik*. Berlin, Germany: Springer, 1986, doi: 10.1007/978-3-642-61633-4.
[21] Y. Fu, P. Zhang, J. P. Verboncoeur, and X. Wang, "Electrical breakdown from macro to micro/nano scales: A tutorial and a review of the state of the art," *Plasma Res. Exp.*, vol. 2, no. 1, Feb. 2020, Art. no. 013001, doi: 10.1088/2516-1067/ab6c84.
[22] T. Kammermann, L. Merotto, D. Bleiner, and P. Soltic, "Spark-induced breakdown spectroscopy for fuel-air equivalence ratio measurements at internal combustion engine-relevant conditions," *Spectrochimica Acta B, At. Spectrosc.*, vol. 155, pp. 79–89, May 2019, doi: 10.1016/j.sab.2019.03.006.
[23] P. A. Anderson, "The work function of copper," *Phys. Rev.*, vol. 76, no. 3, pp. 388–390, Aug. 1949, doi: 10.1103/PhysRev.76.388.
[24] N. Barrett, O. Renault, H. Lemaître, P. Bonnaillie, F. Barcelo, F. Miserque, M. Wang, and C. Corbel, "Microscopic work function anisotropy and surface chemistry of 316L stainless steel using photoelectron emission microscopy," *J. Electron Spectrosc. Rel. Phenomena*, vol. 195, pp. 117–124, Aug. 2014, doi: 10.1016/j.elspec.2014.05.015.
[25] G. J. M. Hagelaar, "Brief documentation of BOLSIG+ version 03/2016," Lab. Plasma Convers. d'Energie, Univ. Paul Sabatier, France, Tech. Rep., Mar. 2016, p. 21.
[26] (Jun. 4, 2013). *SIGLO Database*. [Online]. Available: http://www.lxcat.laplace.univ-tlse.fr
[27] (Jun. 4, 2013). *PHELPS Database*. [Online]. Available: http://www.lxcat.laplace.univ-tlse.fr
[28] (Jun. 4, 2013). *MORGAN Database*. [Online]. Available: http://www.lxcat.laplace.univ-tlse.fr
[29] R. H. Fowler and L. Nordheim, "Electron emission in intense electric fields," *Proc. Roy. Soc. London A, Math., Phys. Eng. Sci.*, vol. 119, pp. 173–181, Mar. 1928.
[30] L. Warne, R. Jorgenson, and S. Nicolaysen, "Ionization coefficient approach to modeling breakdown in nonuniform geometries," Sandia Nat. Laboratories, Albuquerque, MA, USA, Tech. Rep. SAND2003-4078, Nov. 2003, vol. 918222, doi: 10.2172/918222.
[31] F. Llewellyn-Jones and F. Llewellyn-Jones, *Ionization and Breakdown in Gases*. London, U.K.: Methuen, 1966.
[32] D. B. Go, *Ionization and Ion Transport*. SanRafael, CA, USA: Morgan & Claypool Publishers, 2018, doi: 10.1088/978-1-6817-4601-2.
[33] S. Pancheshnyi, "Role of electronegative gas admixtures in streamer start, propagation and branching phenomena," *Plasma Sources Sci. Technol.*, vol. 14, no. 4, pp. 645–653, Nov. 2005, doi: 10.1088/0963-0252/14/4/002.
[34] J. G. Trump, R. W. Cloud, J. G. Mann, and E. P. Hanson, "Influence of electrodes on D-C breakdown in gases at high pressure," *Electr. Eng.*, vol. 69, no. 11, pp. 961–964, Nov. 1950, doi: 10.1109/EE.1950.6437081.
[35] B. G. Baker, B. B. Johnson, and G. L. C. Maire, "Photoelectric work function measurements on nickel crystals and films," *Surf. Sci.*, vol. 24, no. 2, pp. 572–586, Feb. 1971, doi: 10.1016/0039-6028(71)90282-2.
[36] H. B. Mann and D. R. Whitney, "On a test of whether one of two random variables is stochastically larger than the other," *Ann. Math. Statist.*, vol. 18, no. 1, pp. 50–60, Mar. 1947, doi: 10.1214/aoms/1177730491.

MICHELANGELO BALMELLI was born in Sorengo, Ticino, Switzerland, in 1992. He received the B.Sc. and M.Sc. degrees in mechanical engineering from ETH Zürich, Zürich, Switzerland. He is currently pursuing the joint Ph.D. degree with the Automotive Powertrain Technology Laboratory, Empa, Dübendorf, Switzerland, and the Laboratory High-Power Electronic Systems, ETH Zürich. His current research interests include pulsed gas discharge physics, plasma-assisted ignition and combustion, and solid-state pulse generators.

YANG LU was born in Hohhot, Nei Mongol, China, in 1994. He received the master's degree (Hons.) in physics from the University of Oxford, U.K., in 2018, and the M.Sc. degree in energy science and technology from ETH Zürich, Zürich, Switzerland, in 2021, where he is currently pursuing the Ph.D. degree with the High Voltage Laboratory.

His current research interest includes corona noise emission on power line conductors.

RAPHAEL FÄRBER received the M.Sc. degree in physics from the Ecole Polytechnique Fédérale de Lausanne (EPFL), Switzerland, and the Ph.D. degree from ETH Zürich, Switzerland. He is currently a Postdoctoral Researcher with the High Voltage Laboratory, ETH Zürich. His research interests include the characterization and understanding of charge transport in solid and gaseous dielectrics, with a current focus on partial discharge phenomena under transient voltages.

LAURA MEROTTO received the M.S. degree and the Ph.D. degree in aerospace engineering from the Politecnico di Milano, Italy, in 2005 and 2011, respectively.

From 2007 to 2013, she was a Research Assistant and a Teaching Assistant with the Aerospace Engineering Department, Politecnico di Milano, where she focused on the theoretical and experimental investigation of combustion processes on hybrid rocket engines, and on innovative formulations of solid fuels for hybrid aeronautical and space applications. From 2014 to 2017, she was a Researcher at CNR—Istituto di Chimica della Materia Condensata e di Tecnologie per l'Energia, Milano, Italy, where she was a Project Leader of Fundamental Investigation on Flames Using Optical Techniques (Chemiluminescence and LIBS) and Thermoelectric Power Generation. In 2018, she joined Empa (Swiss Federal Laboratories for Materials Science and Technology, Switzerland), where she is currently the Project Leader of SIBS-Based Diagnostics for Ignition. Her research interests include innovative ignition concepts (nanosecond repetitively pulsed ignition, NRPD) on methane and methane/hydrogen mixtures for internal combustion engines.

Dr. Merotto is an Active Member of the Combustion Institute and has authored more than 40 publications in books and international journals. Her awards and honors include the American Institute of Aeronautics and Astronautics (AIAA) Best Paper 2011, the ITWIIN (Association of Italian Women for Invention and Innovation) 2012 Award for Best Innovation for Green, Low Cost Mass Access to Space, and the International Prize "Premio Verde Ambiente 2013" for the effort in developing environmental friendly technology solutions.

PATRIK SOLTIC (Member, IEEE) received the Dipl. (Ing.) (ETH) degree in mechanical engineering and the Dr.Sc. (ETH) degree in mechanical engineering (technology) from ETH Zürich, Switzerland, in 1996 and 2000, respectively.

He leads the research activities on energy converters with the Automotive Powertrain Technologies Laboratory and the Swiss Federal Laboratories for Materials Science and Technology (Empa). His research of the group focuses mainly on efficient and low-pollution use of renewable fuels in internal combustion engines. Since renewable fuels often demand for high ignition energies to establish robust flame propagation, he established the research field of ignition in his group's activities. He is the (co)author of more than 100 articles and holds four patents in the field of injection and variable gas exchange. He was awarded the Clifford S. Steadman Prize of IMechE for his Ph.D. thesis, in 2001.

DAVIDE BLEINER was born in Rome, Italy, in February 1973. He received the Laurea degree in earth sciences, in 1998, and the Ph.D. degree in chemistry from ETH Zürich (Group D. Günther) working on laser ICP-MS microanalysis, in 2002.

He did his first postdoctoral research with the Empa National Laboratories in Analytical Chemistry to expand his experience with a larger number of analytical techniques. He did his second postdoctoral research in Belgium on plasma modeling for analytical chemistry (Group A. Bogaerts). In 2007, he got appointed Oberassistent at ETH Zürich (engineering) on a program about laser plasma Extreme Ultraviolet emission. In 2011, he was awarded the SNSF Professorship with the University in Bern, to develop applications for X-ray Lasers. Finally, he got an appointment as the Head of the Division of the Advanced Analytical Technologies with the Empa National Laboratories, in 2014. His focus is in enabling tabletop or portable analysis methods to address pressing problem in the industry and society.

JÜRGEN BIELA (Senior Member, IEEE) received the Diploma degree (Hons.) from Friedrich-Alexander Universität Erlangen-Nürn berg, Erlangen, Germany, in 1999, and the Ph.D. degree from the Swiss Federal Institute of Technology (ETH), Zürich, Switzerland, in 2006. In 2000, he joined the Research Department, Siemens A&D, Erlangen, and in 2002, he joined the Power Electronic Systems Laboratory, ETH Zürich, as a Ph.D. Student focusing on electromagnetically integrated resonant converters, where he was a Postdoctoral Fellow, from 2006 to 2010. Since 2010, he has been an Associate Professor, and since 2020, a Full Professor in high-power electronic systems with ETH Zürich.

CHRISTIAN M. FRANCK (Senior Member, IEEE) received the Diploma degree in physics from the University of Kiel, Germany, in 1999, and the Ph.D. degree in physics from the University of Greifswald, Germany, in 2003. From 2003 to 2009, he was with the ABB Swiss Corporate Research Center, Baden, Dättwil, Switzerland, as a Scientist and a Group Leader in gas circuit breakers and high-voltage systems. He is currently a Full Professor in high-voltage technology with ETH Zürich, Switzerland. His current research interests include gaseous and solid insulation systems and switching arcs.